

$^{130}\text{Te}_2$ spectroscopic reference for neutral Ti lines at 391 nm and 498 nm

MATTHEW BILOTTA,^{1,2,*} LUIS CASTILLO GONZÁLEZ,^{1,2} SCOTT EUSTICE,^{1,2} JACKSON SCHROTT,^{1,2} AND DAN M. STAMPER-KURN^{1,2,3}

¹*Department of Physics, University of California, Berkeley, CA 94720*

²*Challenge Institute for Quantum Computation, University of California, Berkeley, CA 94720*

³*Materials Sciences Division, Lawrence Berkeley National Laboratory, Berkeley, CA 94720*

Present address (M.B.): Department of Physics, Harvard University, Cambridge, MA 02138

Present address (L.C.G.): Universitat Autònoma de Barcelona (UAB), 08193 Bellaterra, Barcelona, Spain

Present address (S.E.): Joint Quantum Institute, National Institutes for Standards and Technology, College Park, MD 20742

**mbilotta@g.harvard.edu*

Abstract: We report on the use of ditellurium ($^{130}\text{Te}_2$) as a frequency reference for laser locking at 391 nm and 498 nm optical wavelengths, which are of interest in titanium (Ti) laser-cooling experiments. In the ultraviolet region near the optical wavelength of 391 nm, 36 previously unobserved transitions were found using laser absorption spectroscopy in a 256 GHz range. Based on the established molecular structure of $^{130}\text{Te}_2$, we attribute these lines to the $0_u^+ \rightarrow 0_g^+$ subsystem of the $^3\Sigma_u^- \rightarrow ^3\Sigma_g^-$ transition with possible vibrational transitions of $\nu = (28, 27, 26, 25, 24) \rightarrow 0$ and $(27, 26) \rightarrow 1$. We measure the frequencies of these lines, and also of lines near 498 nm wavelength, and subsequently stabilize lasers at wavelengths of 391 nm (and 498 nm) to ~ 60 MHz (~ 50 MHz) wide resonances in $^{130}\text{Te}_2$, near the optical-pumping (laser-cooling) transitions in ^{48}Ti . We observe robust laser frequency locks, with Allan deviations of 4.9×10^{-10} (3.6×10^{-11}) at 10 s of averaging time for the 391 nm (498 nm) wavelength lasers.

1. Introduction

Molecular absorption spectroscopy is a widely used, practical route to absolute laser-frequency referencing across many areas of physics, chemistry, and optical engineering. In this approach, a laser is locked by comparing its frequency to a stable molecular transition and feeding back to a tuning actuator, yielding long-term stability without the cost and complexity of frequency combs or ultra-low expansion reference cavities. In contrast to atomic vapor references, which offer sparse resonances and can be difficult or impractical to realize with sufficient optical depth for some elements (e.g., refractory metals), molecules are furnished with dense forests of narrow lines arising from electronic, vibrational, and rotational structure, providing many convenient lock points. A few molecular species are widely used as frequency references in different spectral regions, notably iodine (I_2), hydrogen fluoride (HF), carbon monoxide (CO), and acetylene (C_2H_2). Extensive spectroscopic data is available for these species [1–4].

One limitation of molecular references is that they become unsuitable below a cut-off wavelength due to photodissociation of the molecules, limiting the use of such references for stabilizing visible and ultraviolet lasers. The iodine dimer, for instance, only has usable resonances at optical wavelengths longer than ~ 500 nm [5].

A molecular reference known to provide transitions below the dissociation limit of iodine is ditellurium (Te_2). In particular, Te_2 exhibits a dense set of absorption lines between its ground X state and the excited A and B states, spanning optical wavelengths of 381–534 nm as identified from photographic absorption spectra of hot gaseous Te_2 [6]. Light in this wavelength range has myriad uses, such as laser cooling and trapping of alkaline-earth atoms and ions [7–9], resonance-enhanced photoionization for isotope-selective ion-trap loading [10, 11],

and fluorescence-based state detection for trapped-ion and neutral atom quantum information experiments [12, 13]. The early film-based spectroscopy on Te_2 provided line positions and intensities with large uncertainties, especially near the ultraviolet limit. More recently, vapor cells containing isotopically pure $^{130}\text{Te}_2$ have been used in precision laser spectroscopy studies, but these studies have been limited to wavelengths above $\lambda = 410$ nm [14, 15].

In this work, we carry out Doppler-broadened and Doppler-free laser absorption spectroscopy on a vapor of $^{130}\text{Te}_2$ across a 256 GHz frequency range near an optical wavelength of 391 nm, identifying 36 previously unobserved resonances. Motivated by the need to stabilize lasers near the optical-pumping transition in atomic titanium (Ti) [16, 17], we determine the frequencies of the newly observed $^{130}\text{Te}_2$ resonances relative to the ^{48}Ti optical-pumping line $3d^2 4s^2 a^3F_4 \rightarrow 3d^2(^3P)4s4p(^3P^o) y^5D_4^o$ at $765.666836(3)_{\text{stat}}(30)_{\text{sys}}$ THz (vacuum wavelength of $391.544257(2)_{\text{stat}}(15)_{\text{sys}}$ nm) [16]. Additionally, in agreement with previously published spectra [18], we identify a $^{130}\text{Te}_2$ resonance located near the ^{48}Ti laser-cooling transition $3d^3(^4F)4s a^5F_5 \rightarrow 3d^3(^4F)4p y^5G_6^o$ at $601.615883(3)_{\text{stat}}(30)_{\text{sys}}$ THz (vacuum wavelength of $498.312073(3)_{\text{stat}}(25)_{\text{sys}}$ nm). We measure the offsets between the $^{130}\text{Te}_2$ and ^{48}Ti resonances by simultaneously measuring Doppler-free spectra in the $^{130}\text{Te}_2$ vapor cell and a hollow cathode lamp (HCL) containing atomic Ti. Finally, using frequency modulation (FM) modulation transfer spectroscopy (MTS), we generate error signals from these $^{130}\text{Te}_2$ resonances and perform proportional-integral (PI) feedback to lock the laser frequency. We then evaluate the resulting laser frequency locks, demonstrating their suitability for long-term frequency stabilization.

2. Broadband $^{130}\text{Te}_2$ spectroscopy near 391 nm wavelength

With the goal of finding resonance features at lower wavelengths than the previous blue limit of $\lambda = 410$ nm, we begin by performing high-resolution laser absorption spectroscopy on $^{130}\text{Te}_2$ at wavelengths near 391 nm. Figure 1 shows the layout of the optical setup. Laser light at 391 nm optical wavelength is produced by a Moglabs, Littrow configuration external cavity diode laser (ECDL). An isotopically pure $^{130}\text{Te}_2$ vapor cell rests in the center of our spectroscopy setup and is resistively heated in a furnace. The temperature is adjustable from 500 °C to 900 °C. At these temperatures and wavelengths, the $^{130}\text{Te}_2$ vapor exhibits substantial Doppler broadening, from 0.95 GHz to 1.2 GHz. To resolve the positions of resonances to a precision better than the Doppler linewidth, we employ Doppler-free spectroscopy via counter-propagating pump-probe spectroscopy. Identical spectroscopy is performed simultaneously on a Ti HCL so that all $^{130}\text{Te}_2$ resonance frequencies are measured relative to the measured ^{48}Ti resonance.

To improve the signal-to-noise ratio (SNR) of the Doppler-free features, an MTS scheme is implemented: amplitude modulation (AM) is applied to the pump beam using an optical chopper at 6 kHz, and lock-in detection is performed on the probe beam signal [19]. Additionally, the cell temperature is tuned to optimize the SNR of the demodulated MTS signal. For spectroscopy, we choose 600 °C, as it maximizes the SNR of the MTS signal at the resonance closest to the $a^3F_4 \rightarrow y^5D_4^o$ optical-pumping transition in Ti. See appendix S1 for further details on the temperature dependence of our observations.

Frequency sweeps of the 391 nm light are performed by driving the slow cavity piezo within the ECDL. The laser frequency is determined using a High-Finesse wavemeter. We observe ~ 3 MHz drifts of our wavemeter calibration on 10 min timescales, which is a systematic uncertainty in the relative frequencies of all the lines we measure in this study. The data acquisition from the wavemeter and the spectroscopy traces are synchronized to the laser scan, ensuring that the recorded signals are referenced consistently across all scans. The wavemeter is calibrated to a laser locked to the ^{87}Rb D_2 line (wavelength 780 nm). During the individual frequency scans, the laser output power varies by roughly 50%. To eliminate the impact of these power variations on the spectra, we measure cell transmission with an autobalanced photoreceiver, which corrects for common-mode intensity noise to the reference and signal ports. This noise-subtracted signal

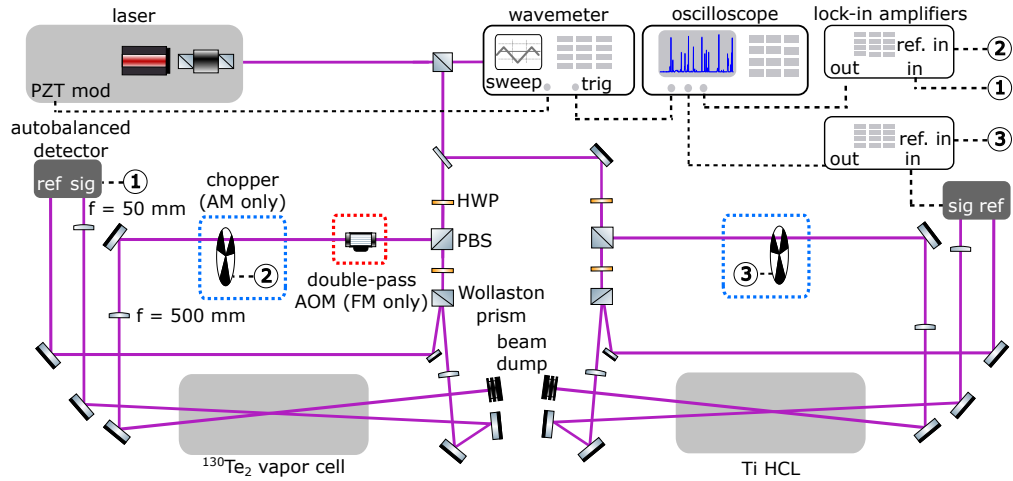


Fig. 1. Experimental setup for $^{130}\text{Te}_2$ and Ti spectroscopy. Light from an external-cavity diode laser is split into pump and probe arms for modulation transfer spectroscopy (MTS). The pump-probe power ratio is set with a half waveplate (HWP) and polarizing beam splitter (PBS). For amplitude modulation (AM) MTS, the probe is detected with an autobalanced receiver referenced to a pick-off beam to suppress common-mode intensity noise; the differential output is recorded during linear frequency sweeps and converted to absorbance. Moreover, the pump is chopped and the signal is demodulated with a lock-in amplifier. For frequency modulation (FM) MTS, the chopper is replaced with a double-pass acousto-optic modulator (AOM) and the autobalanced receiver is replaced with a fast photodiode.

can then be used to determine the absorbance of the $^{130}\text{Te}_2$ vapor.

To explore a large optical frequency band, we carry out a piece-wise scan by adjusting the ECDL grating between segments. In this way, we cover a 256 GHz span between 765.552 THz and 765.808 THz. Figure 2 shows both Doppler-broadened and Doppler-free spectral traces across the full region. Over this span we observe 36 transitions, yielding an average density of approximately one resonance every 7.1 GHz, as listed in Table S1. Compared to I_2 , $^{130}\text{Te}_2$ exhibits fewer spectral lines due to the absence of hyperfine structure from its $I = 0$ nuclear spin.

Across the same 256 GHz range, Doppler-free signals are recorded and analyzed. We fit each absorbance trace to a sum of Gaussian functions, with the number of Gaussians chosen to match the number of resolvable transitions above the noise floor. While Doppler broadening is substantially reduced in MTS, the observed linewidths remain broadened by several mechanisms. In our data, the measured MTS full-width at half-maximum (FWHM) values range from approximately 35 MHz to 250 MHz (Table S1). We believe the dominant contributions to this broadening are pressure broadening, which is enhanced by the high vapor-cell temperature, and residual Doppler broadening arising from a nonzero pump-probe crossing angle. For our operating conditions, the pressure-broadened contribution is estimated to be 18(6) MHz FWHM [21], and the residual Doppler broadening is estimated as $\leq 29(7)$ MHz using $\nu_{\text{rD}} = \nu_{\text{D}} \sin(\theta/2)$, where θ is a conservative upper-limit measurement of the pump-probe crossing angle [22]. By comparison, other broadening mechanisms are much smaller: the transit-time broadening is 0.22 MHz for a beam waist of 0.6 mm, and the power broadening is expected to be minor relative to the observed linewidths based roughly on previously reported $^{130}\text{Te}_2$ saturation intensities on similar transitions [7]. Thus, the narrowest observed MTS features are fairly consistent with the combined effect of pressure and residual Doppler broadening. Some resonances are nevertheless substantially broader than 35 MHz; in those cases, we cannot determine with certainty whether the

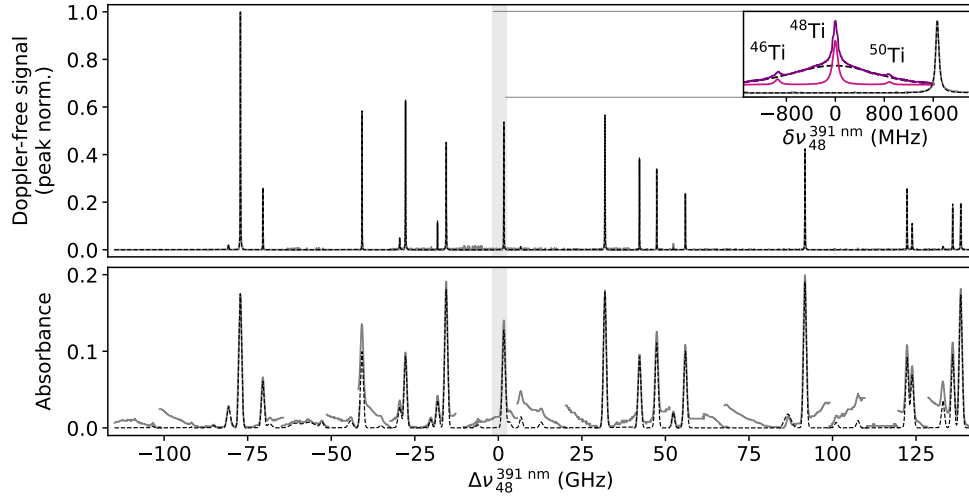


Fig. 2. Doppler-broadened and saturated absorption spectrum of $^{130}\text{Te}_2$ (dark grey) over 256 GHz scan at 600 °C. The frequency axis is defined relative to the absolute frequency of the $a^3F_4 \rightarrow y^5D_4^o$ line used for optical-pumping of ^{48}Ti at $\lambda = 391$ nm. The total spectrum is the result of a piece-wise concatenation of 26 different scans, resulting in 36 total transitions (Table S1). Transitions are determined by fitting each piece-wise scan to a sum of Gaussians plus a linear offset to account for an etalon. The inset shows the MTS signal of $^{130}\text{Te}_2$ (dark grey) near the MTS spectrum of the $a^3F_4 \rightarrow y^5D_4^o$ optical-pumping transition of Ti at 391 nm (dark purple). The Ti spectrum is fit with 3 Lorentzians added atop a Gaussian background. The fit of the 3 Lorentzians (light purple) shows clear peaks for the three $I = 0$ isotopes of Ti (^{46}Ti , ^{48}Ti , ^{50}Ti). The Gaussian background (black, dashed line) is produced by velocity-changing collisions between the HCL buffer gas and the Ti atoms excited by the pump [20]. A small vertical offset is applied between the two spectra for clarity. For this work, we define absorbance as $\log_{10}(P_{\text{in}}/P_{\text{out}})$, where P_{in} and P_{out} are the input and output optical powers from the vapor cell, respectively.

observed feature corresponds to a single broad resonance or to multiple overlapping resonances.

Based on the established molecular structure, the observed features belong to the $0_u^+ \rightarrow 0_g^+$ subsystem of the $^3\Sigma_u^- \rightarrow ^3\Sigma_g^-$ transition [6]. By comparing with band-head data [23], we infer that the observed lines have possible vibrational assignments of $\nu = (28, 27, 26, 25, 24) \rightarrow 0$ and $(27, 26) \rightarrow 1$. The states are well described by Hund's case (c) due to strong spin-orbit coupling, with good quantum numbers Ω , J_e , and J . The upper and lower electronic states are referred to as $\text{B}0_u^+$ and $\text{X}0_g^+$, respectively. Uncertainties in the rovibrational molecular constants and spectral perturbations from molecular level crossings preclude a more precise rovibrational transition assignment. Further discussion of our fitting and assignment of the $^{130}\text{Te}_2$ lines is given in appendix S2.

This wide-range survey furnishes the frequency map needed for targeted laser stabilization. In the next section we focus on resonances near the Ti optical-pumping and laser-cooling transitions, at wavelengths of 391 nm and 498 nm.

3. Laser locking using $^{130}\text{Te}_2$ references to address Ti optical resonances

We now consider a specific application of the $^{130}\text{Te}_2$ vapor frequency references: stabilizing lasers close in frequency to the laser cooling and optical pumping transitions in ^{48}Ti . Toward

this aim, we identify molecular transitions whose optical frequencies lie within several GHz of the relevant Ti atomic transitions—mindful that the remaining frequency offset between the $^{130}\text{Te}_2$ and Ti resonances can be spanned by GHz-range electro-optical modulation or offset locks—and for which we observe strong, Doppler-free molecular resonances in the MTS signal. From the spectroscopy in the preceding section, we identify a $^{130}\text{Te}_2$ resonance at $765.668495(10)_{\text{stat}}(30)_{\text{sys}}$ THz with a MTS linewidth of $63.0(7)$ MHz that lies $1.659(10)$ GHz above the $a^3F_4 \rightarrow y^5D_4^0$ optical-pumping transition of Ti at 391 nm wavelength (see the inset of Fig. 2 and Table S1 in appendix S2). Using existing spectra as a guide [15, 18], we also identify a $^{130}\text{Te}_2$ absorption feature in the vicinity of the Ti cooling transition at 498 nm wavelength. Fig. 3 shows simultaneously measured AM MTS spectra of this line and the laser-cooling transition in Ti. From these spectra we measure a frequency offset of $\delta\nu_{48}^{498\text{ nm}} = -299.5(1)$ MHz between the $^{130}\text{Te}_2$ and ^{48}Ti lines, and an MTS linewidth of $50.5(3)$ MHz for the $^{130}\text{Te}_2$ resonance.

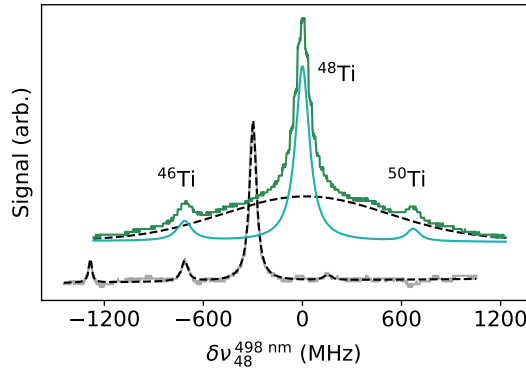


Fig. 3. Amplitude-modulated spectrum of $^{130}\text{Te}_2$ (light grey) at 725°C and saturated absorption spectrum of Ti (dark green) at $\lambda = 498$ nm. The frequency axis is defined relative to the absolute frequency of the $^{48}\text{Ti } a^5F_5 \rightarrow y^5G_6^0$ line used for cooling. The fit of 3 Lorentzians (light green) shows clear peaks for the three $I = 0$ isotopes ($^{46}\text{Ti}, ^{48}\text{Ti}, ^{50}\text{Ti}$) by subtracting from the Ti signal the Gaussian background (black, dashed line) that is produced by velocity-changing collisions of atoms that are excited by the pump [20]. The $^{130}\text{Te}_2$ signal is fitted with 4 Lorentzians (black, dashed line). A small vertical offset is applied between the two spectra for clarity.

Having identified $^{130}\text{Te}_2$ resonances near the relevant Ti transitions, we next lock the laser frequency to these molecular spectroscopy features. To generate an error signal for stabilization, we implement FM MTS by replacing the optical chopper with a double-pass AOM in the pump path (see Fig. 1). To accommodate the higher detection bandwidth required for FM operation, we also replace the autobalanced receiver with a fast photodiode while keeping the pump-probe geometry unchanged. The AOM is driven by a voltage-controlled oscillator (VCO) whose frequency is dithered at 145 kHz, with the modulation parameters adjusted to maximize the error-signal slope while maintaining a high signal-to-noise ratio. The double-pass configuration also provides a convenient fixed frequency offset between the lock point and the transition center.

The lock performance is quantified on short timescales by monitoring the power spectral density of the feedback error signal and on long timescales by reference to a wavemeter. At 391 nm wavelength, we obtain robust locks, with a long-term frequency distribution characterized by a Gaussian width of 5.5 MHz (Fig. 4(b)); the capture range of the error signal is approximately 25.8 MHz (Fig. 4(a)). Relative to the unlocked case, we found that the drift over a 4-hour span is reduced by a factor of about 30. At 498 nm wavelength, the $^{130}\text{Te}_2$ -referenced lock exhibits a Gaussian frequency width of 0.2 MHz (Fig. 4(b)), with an observed capture range of

29.8 MHz (Fig. 4(a)). These results demonstrate that the identified $^{130}\text{Te}_2$ resonances provide stable, high-contrast error signals suitable for long-term operation near both Ti transitions.

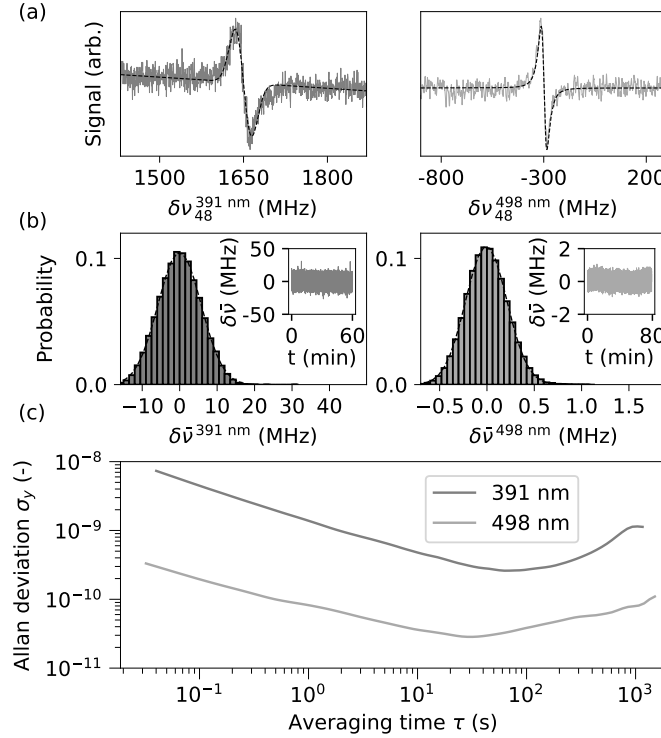


Fig. 4. (a) Error signals of the actively locked lasers at 391 nm (dark grey) and 498 nm (light grey), obtained by demodulating MTS signals from the $^{130}\text{Te}_2$ vapor cell with a lock-in amplifier. Before the cell, which was held at 600 °C for the 391 nm measurement and at 725 °C for the 498 nm measurement, the 391 nm laser was operated with probe and pump powers of 0.31 mW and 0.85 mW, respectively, whereas the 498 nm laser used 0.15 mW (probe) and 21.2 mW (pump). The frequency axes are defined relative to the ^{48}Ti optical-pumping line $a^3F_4 \rightarrow y^5D_4^o$ and the ^{48}Ti laser-cooling transition $a^3F_4 \rightarrow y^5G_6^o$, respectively. Both signals are fitted to the derivative of a Lorentzian plus a linear background (black, dashed lines). (b) Histograms of frequency deviations from the mean of each actively locked laser, fitted to a Gaussian (black, dashed line). The insets show the corresponding long-term frequency scans with respect to the mean laser frequency. (c) Allan deviation of the actively locked lasers, showing their fractional frequency stability as a function of averaging time. See appendix S3 for further details on the calculation of the Allan deviation.

Fig. 4(c) plots the Allan deviation of the frequency of the locked lasers. The data reveals that the 498 nm lock provides better fractional frequency stability than the 391 nm lock over the full range of averaging times. At short averaging times, both traces follow the expected $\sigma_y \propto \tau^{-1/2}$ scaling of white-frequency noise, consistent with noise in the lock signal dominating the short-term stability. Each curve reaches a clear minimum and then turns upward at long averaging times, indicating the onset of slower correlated noise processes and drift. The 498 nm lock reaches a lower minimum than the 391 nm lock, consistent with higher effective SNR and reduced sensitivity to environmental noise and drift. Although the 391 nm lock is less stable overall, its correct short-term scaling and well-defined minimum suggest that the remaining

limitation is primarily technical rather than fundamental.

4. Conclusion

In summary, we have demonstrated that $^{130}\text{Te}_2$ provides a set of reliable frequency references for laser stabilization in the ultraviolet and visible regimes, in particular at lower optical wavelengths than the previously observed wavelength limit of 410 nm [14, 15, 18]. We demonstrate that these frequency references provide convenient locking points for lasers used to drive atomic resonances in Ti, relevant to optical pumping and laser cooling. Numerous other applications in the same wavelength range can also be pursued.

Funding. This material is based upon work supported by the U.S. Department of Energy, Office of Science, National Quantum Information Science Research Centers, Quantum Systems Accelerator. Additional support is acknowledged from the ONR (Grants No. N00014-20-1-2513 and No. N00014-22-1-2280), the ARO (Grants No. W911NF2010266 and No. W911NF2310244), and the NSF (PHY-2012068 and the QLCI program through Grant No. OMA-2016245). L.C.G. acknowledges funding from the UAB Exchange Programme, the University of California Education Abroad Program (UCEAP) and the MOBINT-MIF Scholarship from AGAUR.

Acknowledgment. We thank Professor Amanda Ross for insightful discussions regarding the band assignment of ditellurium lines in the spectroscopy.

Disclosures. The authors declare no conflicts of interest.

Data Availability. Data underlying the results presented in this paper are not publicly available at this time but may be obtained from the authors upon reasonable request.

Supplemental document. See supplement for supporting content.

References

1. S. Gerstenkorn and P. Luc. *Atlas du spectre d'absorption de la molécule d'iode 14800-20000 cm⁻¹*. 1978.
2. Shailendhar Saraf, Paul Berceau, Alberto Stochino, Robert Byer, and John Lipa. Molecular frequency reference at $1.56\mu\text{m}$ using a $^{12}\text{C}^{16}\text{O}$ overtone transition with the noise-immune cavity-enhanced optical heterodyne molecular spectroscopy method. *Opt. Lett.*, 41(10):2189–2192, May 2016.
3. Petr Balling, Marc Fischer, Philipp Kubina, and Ronald Holzwarth. Absolute frequency measurement of wavelength standard at 1542 nm: acetylene stabilized DFB laser. *Opt. Express*, 13(23):9196–9201, Nov 2005.
4. Shizuo Yamaguchi and Masao Suzuki. Frequency locking of an InGaAsP semiconductor laser to the first overtone vibration-rotation lines of hydrogen fluoride. *Applied Physics Letters*, 41(11):1034–1036, 12 1982.
5. Wang-Yau Cheng, Lisheng Chen, Tai Hyun Yoon, John L. Hall, and Jun Ye. Sub-doppler molecular-iodine transitions near the dissociation limit (523 – 498nm). *Opt. Lett.*, 27(8):571–573, Apr 2002.
6. R. F. Barrow and R. P. du Parcq. Rotational analysis of the $\text{A } 0_u^+ \text{, B } 0_u^+ \text{-X } 0_g^+$ systems of gaseous Te_2 . *Proceedings of the Royal Society of London. A. Mathematical and Physical Sciences*, 327(1569):279–287, March 1972.
7. Jennifer Taylor, Bryan Hemingway, James Hanssen, Thomas B. Swanson, and Steven Peil. Vapor-cell frequency reference for short-wavelength transitions in neutral calcium. *J. Opt. Soc. Am. B*, 35(7):1557–1562, Jul 2018.
8. T. G. Akin, Bryan Hemingway, and Steven Peil. Tellurium spectrometer for $^1\text{S}_0\text{-}^1\text{P}_1$ transitions in strontium and other alkaline-earth atoms. *Review of Scientific Instruments*, 93(5):053002, 05 2022.
9. Tarun Dutta, Debashis De Munshi, and Manas Mukherjee. Absolute Te_2 reference for barium ion at 455.4 nm. *J. Opt. Soc. Am. B*, 33(6):1177–1181, Jun 2016.
10. D. M. Lucas, A. Ramos, J. P. Home, M. J. McDonnell, S. Nakayama, J.-P. Stacey, S. C. Webster, D. N. Stacey, and A. M. Steane. Isotope-selective photoionization for calcium ion trapping. *Phys. Rev. A*, 69:012711, Jan 2004.
11. M. Johanning, A. Braun, D. Eiteneuer, Chr. Paape, Chr. Balzer, W. Neuhauser, and Chr. Wunderlich. Resonance-enhanced isotope-selective photoionization of YbI for ion trap loading. *Applied Physics B*, 103:327–338, 2011.
12. F. Schmidt-Kaler, S. Gulde, M. Riebe, T. Deuschle, A. Kreuter, G. Lancaster, C. Becher, J. Eschner, H. Häffner, and R. Blatt. The coherence of qubits based on single Ca^+ ions. *Journal of Physics B: Atomic, Molecular and Optical Physics*, 36(3):623, January 2003.
13. Alec Jenkins, Joanna W. Lis, Aruku Senoo, William F. McGrew, and Adam M. Kaufman. Ytterbium nuclear-spin qubits in an optical tweezer array. *Physical Review X*, 12(2):021027, 2022.
14. I.S. Burns, J. Hult, and C.F. Kaminski. Use of $^{130}\text{Te}_2$ for frequency referencing and active stabilisation of a violet extended cavity diode laser. *Spectrochimica Acta Part A: Molecular and Biomolecular Spectroscopy*, 63(5):905–909, April 2006.
15. Amanda J. Ross and Joseph M. Cardon. Te_2 absorption spectrum from 19000 to 24000 cm^{-1} . *Journal of Molecular Spectroscopy*, 384:111589, 2022.

16. Scott Eustice, Jackson Schrott, Anke Stöltzel, Julian Wolf, Diego Novoa, Kayleigh Cassella, and Dan M. Stamper-Kurn. Magneto-optical trap of titanium atoms. *Phys. Rev. Res.*, 7:023025, Apr 2025.
17. Scott Eustice, Dmytro Filin, Jackson Schrott, Sergey Porsev, Charles Cheung, Diego Novoa, Dan M. Stamper-Kurn, and Marianna S. Safronova. Supplemental material for “optical telecommunications-band clock based on neutral titanium atoms”. *Physical Review A*, 107(5):L051102, May 2023.
18. P Luc and J Cariou. *Atlas du spectre d'absorption de la molécule de tellure*. Laboratoire Aime-Cotton CNRS II, Orsay, France, 1980.
19. Jon H. Shirley. Modulation transfer processes in optical heterodyne saturation spectroscopy. *Opt. Lett.*, 7(11):537–539, Nov 1982.
20. Andrew O. Neely, Kayleigh Cassella, Scott Eustice, A A, and Dan M. Stamper-Kurn. Isotope shifts in the metastable a^5F and excited y^5G^o terms of atomic titanium. *Phys. Rev. A*, 103:032818, Mar 2021.
21. Arnolds Ubelis. Temperature dependence of the saturated vapor pressure of tellurium. *Journal of Engineering Physics*, 42:309–315, 03 1982.
22. Isao Hirano. Effect of intersection angle between saturation and probe beams on saturated absorption spectra of the Cs-D2 line. *Journal of Quantitative Spectroscopy and Radiative Transfer*, 40(4):531–537, 1988.
23. B.L. Jha, K.V. Subbaram, and D.Ramachandra Rao. Electronic spectra of $^{130}\text{Te}_2$ and $^{128}\text{Te}_2$. *Journal of Molecular Spectroscopy*, 32(3):383–397, December 1969.

Supplementary Material

$^{130}\text{Te}_2$ spectroscopic reference for neutral Ti lines at 391 nm and 498 nm: supplemental document

S1. Temperature dependence of $^{130}\text{Te}_2$ MTS signals

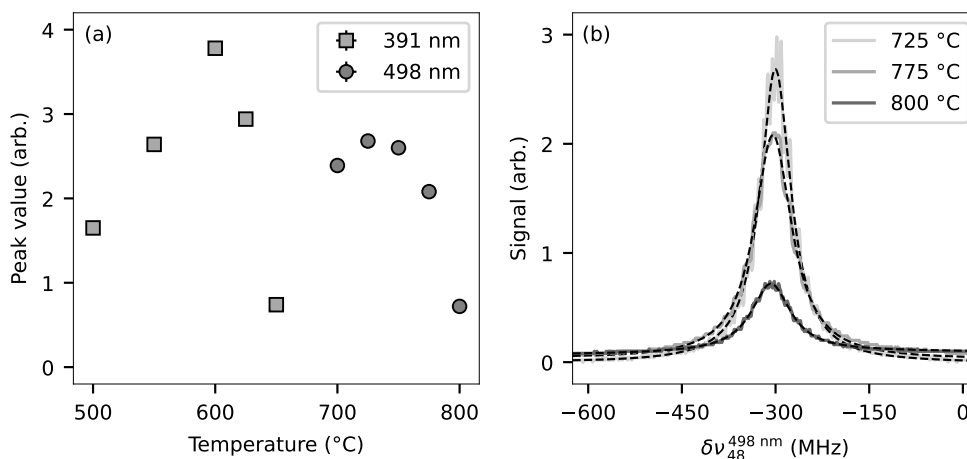


Fig. S1. Temperature dependence of the $^{130}\text{Te}_2$ MTS signal amplitude used for laser spectroscopy. The spectra were recorded while varying the furnace temperature of the $^{130}\text{Te}_2$ vapor cell. Panel (a) shows the $^{130}\text{Te}_2$ MTS peaks, in arbitrary units, at 391 and 498 nm optical wavelengths. The strongest signal, and therefore the highest error-signal SNR, is obtained at 600 °C for 391 nm and 725 °C for 498 nm. Panel (b) shows representative traces of the feature used to lock the laser to the Ti cooling transition at $\lambda = 498$ nm. The signal amplitude reaches a maximum at 725 °C, which is therefore chosen as the operating temperature for locking to this resonance.

To maximize the SNR of the 391 nm and 498 nm optical transitions, we optimized the temperature of the vapor cell in each case. After optimizing at 391 nm, we observe that among the 36 Doppler-broadened absorption features, 21 also exhibit a Doppler-free resonance. At higher temperatures, the pump beam intensity is strongly attenuated as it passes through the cell, reducing the MTS contrast for strong lines, while weaker lines may gain MTS contrast because the higher absorber density compensates for sub-saturation fields. Certain weaker lines, however, may have too low of a transition strength for our laser to sufficiently depopulate the ground state and thus produce an MTS signal. For the 256 GHz scan, we optimize the temperature once for the 765.6685 THz resonance used for locking (Sec. 3), accepting that not all of the transitions will have simultaneously optimal MTS contrast.

S2. Fitting of observed $^{130}\text{Te}_2$ lines and molecular line assignment

Since the dominant form of line-broadening for Doppler-broadened spectroscopy is largely Doppler broadening, we fit each observed line to a Gaussian. MTS spectra are fit to Lorentzian profiles. We also fit the MTS data to Voigt profiles to include both homogeneous and inhomogeneous broadening mechanisms, but found that the data was better fit by a Lorentzian profile. In addition

to the wavemeter-induced 30 MHz uncertainty in the absolute frequency of all lines, we deduce the 1σ statistical uncertainty in fit parameters through diagonal elements in the covariance matrix of the nonlinear least-squares fit. The covariance matrix is estimated from the inverse curvature of the least-squares objective evaluated at the best-fit solution. The Doppler-broadened features are additionally fit with a linear offset per scan to account for an observed etalon with ~ 50 GHz spectral range. Fitting each scan with a broad sinusoidal offset did not yield good fits due to the inter-scan offsets imposed by conversion from photodiode voltage to absolute units of absorbance. We tabulate these fitted line centers and uncertainties in Table S1.

From Sec. 2, we can deduce the electronic subsystem to which the ultraviolet spectroscopy pertains. Furthermore, from prior band-head data [1], we determine that the observed lines reside within the following vibrational transitions: $\nu = (28, 27, 26, 25, 24) \rightarrow 0$ and $(27, 26) \rightarrow 1$. Uncertainties in the rovibrational constants limit a more precise line-by-line assignment. The quoted uncertainty in the rotational constant B_ν ($\pm 5 \times 10^{-6} \text{ cm}^{-1}$) yields an energy uncertainty that scales with $(J^2 + J)$ and corresponds to roughly 12 GHz at high J , while the $\pm 5 \times 10^{-2} \text{ cm}^{-1}$ uncertainty in the vibrational constant ω_ν contributes an additional 8 GHz. Moreover, above $\nu_B = 19$, the vibrational bands exhibit significant perturbations from a linear model $\Delta G(\nu + 1/2)$, thus preventing a more precise vibrational band assignment [1, 2].

S3. Laser lock characterization

We quantify the frequency stability of the frequency-stabilized lasers with the Allan deviation. The wavemeter records wavelength measurements of the actively locked lasers at 391 nm and 498 nm at intervals of $\Delta t = 40$ ms and $\Delta t = 30$ ms, respectively. We convert the recorded wavelengths into optical frequencies and then into fractional frequency deviations,

$$y_i = \frac{\nu_i - \bar{\nu}}{\bar{\nu}}, \quad (\text{S1})$$

where ν_i is the instantaneous frequency corresponding to the i^{th} measurement, and $\bar{\nu}$ is the mean frequency over the full record.

Next, we define 50 logarithmically spaced averaging factors $m \in \mathbb{Z}^+$, ranging from 1 to $m_{\text{max}} = \lfloor N/2 \rfloor$, where N is the total number of measurements. For each m , the corresponding averaging time is $\tau = m\Delta t$, and the averaged fractional frequency is defined as

$$\bar{y}_i(\tau) = \frac{1}{m} \sum_{k=0}^{m-1} y_{i+k}, \quad (\text{S2})$$

where $i \in \{1, 2, \dots, N - m + 1\}$ denotes the index of the first measurement included in the average. Since i increases by one from one average to the next, these averages are formed from overlapping sets of measurements.

For each averaging time τ , the Allan deviation is calculated from the mean squared difference between averaged fractional frequencies separated by m measurements,

$$\sigma_y(\tau) = \sqrt{\frac{1}{2} \langle (\bar{y}_{i+m}(\tau) - \bar{y}_i(\tau))^2 \rangle} = \sqrt{\frac{1}{2L} \sum_{i=1}^L (\bar{y}_{i+m}(\tau) - \bar{y}_i(\tau))^2}, \quad (\text{S3})$$

where $L = N - 2m + 1$ is the number of squared differences included in the average. Each difference compares two adjacent, non-overlapping groups of m measurements, corresponding to a duration τ . Repeating this procedure for all values of m yields the Allan deviation as a function of averaging time.

In Fig. 4(c), for $\tau \leq 3$ s, both locks exhibit $\sigma_y \propto \tau^{-1/2}$ behavior characteristic of white-frequency noise, indicating that random frequency fluctuations from detection noise (including

Doppler Broadened			MTS	
Center (GHz)	FWHM (MHz)	Absorb.	Center (GHz)	FWHM (MHz)
-103.375(36)	–	0.002(1)		
-91.826(37)	–	0.001(1)		
-85.220(6)	–	0.004(3)		
-80.735(13)	1084.4(3.5)	0.006(1)	-80.759(11)	–
-77.188(10)	970.5(1.2)	0.181(3)	-77.158(10)	88.00(61)
-70.456(13)	953.6(3.4)	0.061(4)	-70.432(11)	57.0(1.3)
-68.410(18)	–	0.006(2)		
-60.809(26)	–	0.006(2)		
-56.701(24)	–	0.007(2)		
-52.812(10)	1185(18)	0.007(2)		
-44.269(9)	1425(17)	0.009(2)		
-40.813(10)	1028.5(1.3)	0.099(1)	-40.768(10)	35.00(70)
-35.177(11)	–	0.0036(9)		
-29.506(3)	1094.1(7.6)	0.027(2)	-29.483(10)	165.0(3.5)
-27.767(2)	951.4(2.0)	0.094(2)	-27.746(10)	72.00(55)
-20.264(4)	1049(13)	0.012(2)		
-18.177(10)	962.3(2.0)	0.036(3)	-18.180(10)	39.00(2.0)
-15.609(10)	989.54(0.67)	0.181(4)	-15.585(10)	80.00(0.91)
-6.126(6)	1120(20)	0.004(1)		
1.659(10)	1009.7(2.7)	0.128(2)	1.680(10)	63.00(0.70)
3.338(10)	1216.7(4.7)	0.009(2)		
6.775(10)	883.8(1.4)	0.015(2)	6.692(10)	–
12.819(9)	1132(23)	0.008(2)		
31.897(10)	982.7(1.4)	0.177(4)	31.920(10)	78.00(52)
42.249(10)	997.9(1.8)	0.093(4)	42.254(10)	43.00(54)
47.395(10)	1000.4(1.4)	0.111(4)	47.421(10)	33.00(66)
52.380(10)	880(11)	0.020(3)	52.408(10)	–
55.981(10)	994.2(2.1)	0.100(4)	55.994(10)	51.00(45)
86.626(10)	1039.532(34)	0.018(4)		
91.764(10)	983.3(1.5)	0.191(5)	91.791(10)	75.00(67)
101.090(10)	1090.281(23)	0.007(3)		
107.613(10)	1016.110(17)	0.010(3)		
122.321(10)	973.2(0.91)	0.092(1)	122.337(10)	65.00(91)
123.844(10)	980.1(1.2)	0.069(1)	123.858(10)	81.00(92)
133.044(10)	1027.474(3.1)	0.036(3)	133.164(29)	250.00(85)
135.958(10)	967.2(1.1)	0.096(4)	135.984(10)	81.00(2)
138.384(10)	993.92(0.63)	0.173(5)	138.407(10)	117.00(1.2)

Table S1. Fits of Doppler-broadened and MTS peaks, with statistical uncertainties. The frequencies shown are relative to the $a^3F_4 \rightarrow y^5D_4^o$ optical pumping line at $765.666836(3)_{\text{stat}}(30)_{\text{sys}}$ THz in atomic ^{48}Ti . Some resonances were not seen in MTS, and their corresponding entries are left blank. For particularly weak resonances, we were unable to reliably determine the resonance width, potentially due to the presence of multiple overlapping resonances. The FWHM of these features is indicated by a dash (–). The oscilloscope analog-to-digital converter imparts a 0.001 uncertainty on all peak absorbances, which is greater than the calculated fitting error and thus is reported for all values. At 600 °C, the expected FWHM resulting from Doppler broadening is 1006 MHz, which closely follows the reported widths. Because the amplitudes of the MTS signals depend strongly on the pump power, cell temperature, and system alignment, they are not inherent quantities of the lines. As such, MTS signal amplitude is not tabulated.

shot noise) in the locking system limit the short-term stability. The Allan deviation minima occur at $\sigma_y = 2.8 \times 10^{-11}$ at $\tau = 30$ s for the 498 nm lock and $\sigma_y = 2.6 \times 10^{-10}$ at $\tau = 67$ s for the 391 nm lock. The earlier and lower minimum for 498 nm indicates higher effective SNR and reduced technical or environmental coupling. For $\tau \gtrsim 10^2$ s, both curves turn upward, consistent with random-walk FM and frequency drift, though some portion of the observed uptick may originate from the wavemeter itself through slow drift and infrequent recalibration to our 780 nm reference light. The 391 nm lock shows a stronger rise, indicating larger long-term instabilities. Despite its higher Allan deviation, the 391 nm lock exhibits the expected noise scaling and a clear stability minimum, suggesting that the present performance gap is due to technical imperfections rather than a fundamental limit in the potential lock stability.

References

1. B.L. Jha, K.V. Subbaram, and D.Ramachandra Rao. Electronic spectra of $^{130}\text{Te}_2$ and $^{128}\text{Te}_2$. *Journal of Molecular Spectroscopy*, 32(3):383–397, December 1969.
2. R. F. Barrow and R. P. du Parcq. Rotational analysis of the $A 0_u^+$, $B 0_u^+ - X 0_g^+$ systems of gaseous Te_2 . *Proceedings of the Royal Society of London. A. Mathematical and Physical Sciences*, 327(1569):279–287, March 1972.